Construction and Building Materials 181 (2018) 394–407

Contents lists available at ScienceDirect

Construction and Building Materials

journal homepage: www.elsevier.com/locate/conbuildmat

Nanolime for the consolidation of lime mortars: A comparison of three available products

J. Otero [a,*], V. Starinieri [a], A.E. Charola [b]

[a] Materials and Engineering Research Institute, Sheffield Hallam University, Sheffield S1 1WB, UK
[b] Museum Conservation Institute, Smithsonian Institution, Washington, DC, USA

HIGHLIGHTS

- The consolidation effectiveness of Calosil® and Nanorestore Plus® is reduced with time.
- L'Aquila nanoparticles are more reactive which tend to grow better developed calcites.
- L'Aquila nanolime provides higher durability to dissolution.
- All treatments reduce the porosity in the surface that reduces evaporation rate.
- The whitening effect caused by nanolime treatment is reduced after accelerated weathering.

ARTICLE INFO

Article history:
Received 21 January 2018
Received in revised form 3 May 2018
Accepted 6 June 2018

Keywords:
Nanolime
Nanoparticles
Calcium hydroxide
Consolidation
Limestone
Lime mortar
Calosil
Nanorestore

ABSTRACT

Nanolime products are one of the most promising consolidation methods for historic calcareous substrates. Whilst the popularity of nanolime has been growing, its consolidation mechanism still needs to be fully understood when applied to highly porous substrates. The aim of this paper is to compare the three available nanolime products in terms of consolidation efficacy on lime mortar specimens. It is shown that repeated applications of a low concentrated nanolime can increase the superficial cohesion and the mechanical strength of the mortar within 1 cm from the surface, while also reducing porosity, number of micro-pores and capillary water absorption coefficient. Nanorestore Plus® yielded the highest short-term consolidation effect. However, L'Aquila nanolime showed a higher durability which was attributed to a better developed crystalline structure.

1. Introduction

The consolidation of degraded calcareous materials is one of the main challenges in the conservation of historic structures. Calcareous substrates degrade by weathering processes such as crystallisation of salts, biological activity, freeze-thaw action and chemical attack by acid atmospheric pollutants [1–3]. Consolidants can help in recovering the strength of degraded materials as well as decreasing the deterioration rate of the substrate. In general, suitable consolidants must meet the following criteria: i) be physically, mechanically and chemically compatible with the substrate; ii) have a good adhesion to the substrate; iii) increase the substrate's mechanical properties; iv) not induce colour or aesthetic changes to the substrate; v) reduce porosity but not hamper moisture transport through the substrate. The effectiveness of the consolidation depends on the interaction of a number of factors such as the characteristics of the substrate, the properties of the consolidant and its compatibility with the substrate, and the application methods and conditions [4].

Limewater, which is a saturated solution of calcium hydroxide with a maximum of concentration of 1.5 g/L with lime particles in a colloidal suspension [5], has been used over centuries to consolidate deteriorated limestone or plaster. It has the advantage of being durable and compatible with the substrate as it is based on the precipitation of calcium carbonate into the pores of the treated material by reaction of the calcium hydroxide with the atmospheric carbon dioxide (CO_2). The main constraint of the limewater technique is a low consolidation depth due to limited penetration of carbon dioxide into the substrate [6]. Furthermore, the

* Corresponding author.
E-mail address: b5039083@my.shu.ac.uk (J. Otero).

https://doi.org/10.1016/j.conbuildmat.2018.06.055
0950-0618/

application of limewater can cause whitening of the treated surface. The effectiveness of limewater has been greatly discussed in literature. According to Price et al. [7] when using limewater most particles are deposited within 2 mm from the surface yielding an ineffective consolidation. Price's research has led some stone conservators to be skeptical of this treatment. Nonetheless, Brajer [8] demonstrated that a prolonged uninterrupted application produces a noticeable consolidation effect and some authors brought up new perspectives to its practical work such as the use of lime poultices and of an increased number of limewater applications [3,9,10].

During the last century, organic consolidants (i.e. synthetic polymers, such as Paraloid B-72, Mowilith 30 and Primal AC33) were extensively used in restoration treatments for calcareous materials due to their immediate strength enhancement, ease of application and the limitations shown by limewater [11]. These consolidants proved to be effective in the short and medium term for some calcareous substrates. However, the low compatibility with the mineral substrate and their short durability caused more substrate degradation in the long term, particularly in environments where temperatures increase above 40 °C [3,9,11]. Specifically, physical and mechanical incompatibility between organic consolidants and calcareous substrates can cause crack development, aesthetic changes and interference with future treatments [12,13], sometimes with severe consequences [14,15].

Nanolimes were developed to overcome the limitations of the traditional limewater treatment. Their consolidating effect takes place by the same mechanism as for the limewater technique but the smaller size of the lime particles (nanoscale) improves their performance. The advantages of nanolime compared to limewater are: i) nanolimes contain higher amounts of calcium hydroxide particles; ii) lime nanoparticles are more reactive due to their higher specific surface thus increasing the carbonation rate; iii) nanolimes penetrate deeper into the substrate because of their smaller particle size; iv) nanolimes have better colloidal stability due to their smaller particle size and the electrostatic repulsion forces between them; and, v) reduced whitening of the treated surface when nanolimes are used. An overview of nanolime synthetisation methods and use as a consolidant for calcareous substrates can be found elsewhere [16].

The first nanolime to become available on the market was Calosil® (IBZ-Salzchemie GmbH & Co.KR, Germany) in 2006, followed by Nanorestore® (CSGI – University of Florence, Italy) in 2008. Recently, the University of L'Aquila has patented a new method to synthesise nanolime where nanoparticles are produced by an anion exchange process at ambient room conditions in aqueous suspensions [17–19]. Nanolime produced through this method is currently in the process of being commercialised.

Both Calosil and Nanorestore have been extensively used for the conservation of wall paintings and stuccoes, achieving good readhesion of detached particles or pigment flakes [5,16,20] and consolidating powdering surfaces [15,20]. However, the effectiveness of the nanolimes decreases when mass consolidation of a porous substrate such as deteriorated stone or mortar is required [21–23]. The effectiveness of nanolime as a consolidant appears to be influenced by several factors: i) multiple applications of low nanolime concentration suspensions (i.e. 5 g/L) reduce the accumulation of consolidating product near the surface and improves the yield of carbonation within the pores [24,25]; ii) the type of alcohol used can influence the nanolime deposition in the pores [26,27] as well as the carbonation process [28], iii) external factors such as relative humidity (RH) and exposure time appear to influence the carbonation rate and precipitation of polymorphs [29,30]; iv) age and storing temperature of the nanolime affects the conversion of $Ca(OH)_2$ particles into Ca-alkoxides which can decrease its effectiveness [31].

The aim of this work is to compare the consolidation effectiveness of the three available nanolime products on lime mortars and investigate their long term performance. The influence of the nanolime treatments on mortar superficial cohesion, water absorption by capillarity, drying rate, drilling resistance, pore structure and aesthetic properties have been investigated.

2. Materials and methods

2.1. Lime and sand

Singleton Birch Ultralime CL90 (≥98% $Ca(OH)_2$, measured by XRD and XRF) and silica sand from Pentney (UK) were used throughout this work for the mortar mixes. The sand grading is shown in Fig. 1. The mineralogical composition of the sand, which was determined by XRD (*PANalytical XPert PRO*) using Rietveld refinements, is 96.3% Quartz (SiO_2, ICSD #00-046-1045) and 3.7% Potassium Feldspar ($KAlSi_3O_8$, ICSD #01-076-0831).

2.2. Nanolime

Three nanolime dispersions were used throughout this work:

- **Nanorestore Plus Propanol 5®** (CSGI Consortium – University of Florence, Italy): 5 g/L calcium hydroxide in 2-propanol. Particle size 100–300 nm. This dispersion is referred to as NAN.
- **Calosil IP5®** (by IBZ Salzchemie GmbH & Co.KG, Germany): 5 g/L calcium hydroxide in 2-propanol. Particle size 50–150 nm. This dispersion is referred to as CAL.
- **Nanolime synthesised through the method developed by Taglieri et al [17] at the University of L'Aquila**: 5 g/L calcium hydroxide in 50–50% water – 2-propanol. Particle size 20–80 nm. This dispersion is referred to as LAQ.

LAQ was synthesized through an anionic exchange process carried out at room temperature and ambient pressure by mixing under moderate stirring an anion exchange resin (Dowex Monosphere 550A OH from Dow Chemical) with an aqueous calcium chloride solution following a methodology described by Taglieri et al. [17,18] and Volpe et al. [19]. When these two components are mixed together, the substitution of OH groups in the resin with chloride ions (Cl^-) in solution leads, in conditions of supersaturation, to the formation of pure $Ca(OH)_2$ nanoparticles, following the reaction:

$$CaCl_2 + 2(R\text{ - }OH) \rightarrow Ca(OH)_2 \downarrow + 2(R\text{ - }Cl)$$

The concentration of chloride was monitored during the process (Vernier Chloride Ion-Selective Electrode CL-BTA) and when this

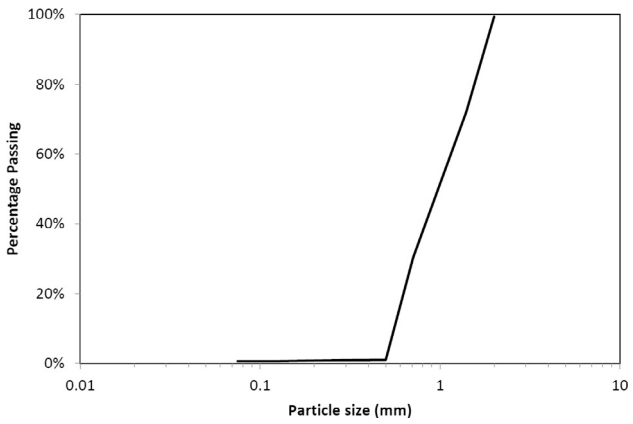

Fig. 1. Sand grading curve.

reached a constant value below 30 mg/L, the stirring was stopped and the aqueous suspension was separated from the resin by means of a sieve (80 μm). The supernatant water was then extracted through a pipette and replaced with 2-propanol in order to maintain a concentration of 5 g/L in a 50–50% vol. water-2-propanol solvent. This is considered the optimal formulation for this nanolime in terms of carbonation and kinetic stability [18,32].

The decrease rate of chloride content during the synthesis was very rapid, with about 97% of the reduction occurring within the first minute of the process. The synthesis was stopped after 15 min when the ion exchange process was completed (zero kinetic exchange), with a total reduction of chloride content of 99.82% and a residual chloride content of 0.18% (29.4 mg/L). Similar results have been reported by Taglieri et al. [17–19,32].

2.3. Mortar preparation and testing

Mortars were produced with a volumetric binder:sand ratio of 1:2.5 to a constant flow of 16 cm measured according to BS EN 1015-3:1999 [33]. Although mix proportions are expressed by volume, mortars were batched by weight after accounting for component densities, which were measured in accordance with BS EN 459-2:2010 [34]. The water:binder ratio was 1.56 to obtain the desired flow. Mortars were produced by mixing the dry ingredients with water in a Hobart mixer. The mix protocol was as follows: 1) dry mix sand and lime for 2 min at 62 rpm; 2) add water while continuing mixing at 62 rpm for 30 s; 3) stop the mixer for 30 s and scrape the mixer bowl; 4) mix for 5 min at 125 rpm. Samples were cast in 40 × 40 × 160 mm steel moulds in two layers and vibration-compacted. Immediately upon floating off the fresh mortar, the moulds were transferred to a temperature and humidity controlled room maintained at 20 °C and 65% RH. Mortar beams were de-moulded after 5 days and stored in the same room for the following 23 days. On the 28th day of curing, each prism was cut into 4 cubes measuring approximately 40 × 40 × 40 mm prior to curing for further 28 days in the same conditions.

The mineralogical composition of the mortar was determined by X-ray Diffraction. Samples obtained from the core of the cube were ground and sieved through an 80 μm sieve mesh and placed over an XRD zero-background sample holder; the XRD patterns were recorded with a step size of 0.026°2θ, in the angular range 5-70°2θ. Quantitative analyses were carried out by means of Rietveld refinement [35,36]. X-ray data were fitted using the pseudo-Voigt profile function. Specimen displacement, polynomial coefficients for the background function, lattice parameters, profile parameters, and Gaussian and Lorentzian profile coefficients were refined. Quantitative analysis by Rietveld refinement shows the mineralogical composition of the mortar is 82.3% Quartz (SiO_2, ICSD #00-046-1045) and 17.7% Calcite ($CaCO_3$, ICSD #00-005-0586).

2.4. Nanolime characterisation

The size, shape and degree of agglomeration of the calcium hydroxide particles in the three nanolime products were determined by TEM (Philips CM200), while the crystalline phase was analysed by XRD. TEM samples were prepared by dispersing 0.2 ml of nanolime suspension in 20 ml of ethanol and placing a few drops of the resulting liquid on a carbon-coated copper grid. XRD samples were prepared by using the zero-background silica sample holder. Both TEM and XRD samples were prepared in nitrogen atmosphere, to prevent carbonation of the lime.

The kinetic stability (KS) of the three products was determined by turbidity measurements, analysing their absorbance at λ = 600 nm by means of a UV/VIS Spectrophotometer (UV–vis Spectrophotometer Varian 50SCAN). Before the test, nanolimes were agitated, instead of sonicated. Sonicating has been the normal practice in previous studies [18,20,26,28], however, agitation was preferred in this work to simulate in-situ conditions where conservators normally have no access to an Ultrasonic Bath. Measurements were taken over a period of up to 2 h. The relative kinetic stability (KS %) was calculated using the following formula:

$$KS\% = 1 - [(A_0 - A_t)/A_0] \times 100$$

where A_0 is the starting absorbance and A_t the absorbance at time t, both at a wavelength of 600 nm [5,28]. KS % decreases as a result of the nanoparticles settling; values range from 0 (unstable dispersion) to 100 (no deposition of nanoparticles).

2.5. Nanolime carbonation process characterisation

The carbonation process was investigated by means of TEM, SEM (SEM, NOVA 200 NanoSEM 450) and XRD. For TEM observations, samples were prepared as described in Section 2.4 and exposed to air for 1 min prior to carrying out the observations. For SEM investigations, 0.10 ml of each suspension were placed on a copper SEM sample holder and exposed to outdoor conditions in a sheltered area (T ≈ 5–15 °C, RH ≈ 60–80%) for 7 days prior to carrying out the observations. SEM micrographs were taken with an ETD detector, a working distance of approximately 3 mm, an optimum accelerating voltage of 15 kV and a spot size of about 30 nm. Specimens were coated with a 20 nm thick layer of gold using a Quorum Q150T coater unit to prevent surface charging.

Samples for XRD were prepared by exposing 0.12 ml of each suspension (NAN, CAL and LAQ) to outdoor conditions in the same sheltered area mentioned previously for 1 h and 7 days prior to analysing by the diffractometer. XRD patterns were recorded in step size of 0.026°2θ. Each experimental diffraction pattern was elaborated by means of a Profile Fit Software (HighScorePlus, PANalytical), and each crystalline phase was identified using the ICSD and ICDD reference databases. Quantitative analyses were carried out by means of Rietveld refinements.

2.6. Nanolime treatment application

Each of the three nanolimes was agitated and applied by brush on the top face (as cast) of three 40 × 40 × 40 mm mortar cubes, allowing the nanolime to be fully absorbed by the mortar between two consecutive brushstrokes. Nanolimes were also agitated between each brushstroke. The treatment was continued until no further absorption was observed for a period of at least one minute after a brushstroke. At this time, the application was interrupted and was repeated 24 h later when the specimen was dry. Samples were weighed before and after each application (after full evaporation of the solvent) to determine the total amount of nanolime absorbed by the mortar. The treatment was considered complete when each mortar cube absorbed 500 mg of calcium hydroxide (approximately 100 ml of nanolime). This required about 20 consecutive days of application for each nanolime. Upon treatment completion, the samples were stored outdoor in the sheltered area for a period of 28 days (T ≈ 5–15 °C, RH ≈ 60–80%). A set of untreated control samples was also stored in the same conditions.

2.7. Evaluation of treatment effectiveness

Following 28-day outdoor exposure, the mortar cubes were dried to constant mass at 60 °C in a fan assisted oven and subsequently stored in a desiccator until testing. The effectiveness of the nanolime was evaluated by means of the tests described below.

The influence of the treatments on pore size distribution and porosity of the mortars was investigated by Mercury Intrusion Porosimetry (MIP) using a PASCAL 140/240 instrument. Each test

was carried out on one fragment measuring approximately 5 × 5 × 10 mm collected within 5 mm from the top surface (as cast) of both treated and control samples. The samples were dried in a fan-assisted oven at 60 °C until constant weight prior to testing. The mercury contact angle was taken to be 140°.

The water absorption coefficient by capillarity (WAC) of both treated and control samples was measured according to EN 13,755 [37]; three samples being tested for each mortar. Upon completion of this test, once asymptotic water absorption was reached, samples were immersed in water for 24 h and their apparent porosity was calculated following ASTM C 97–96 (American Society for Testing and Materials, 1996) [38], although the actual immersion time was half of that recommended in this standard. Their drying behaviour was sequentially calculated according to CEN EN 16,322 [39]. This sequence simulates a real situation in an outdoor condition (cycles of dry-wet-dry).

The influence of the nanolime treatments on the surface cohesion of the mortar was evaluated by means of the 'Scotch Tape Test' (STT) carried out in accordance with ASTM D3359 [40]. The test was performed on both treated and control samples and results taken as the average of 9 measurements per sample.

The consolidation effectiveness of the three nanolimes was also assessed by means of a Drilling Resistance Measurement System (DRMS) from SINT-Technology. The DRMS measures the force required to drill a hole at constant rotation (rpm) and lateral feed rate (mm/min). It is generally considered the most suitable methodology for quantifying consolidation effectiveness and depth of penetration of consolidants, particularly in soft stones [41,42]. Tests were performed on both treated and control mortar cubes using drill bits of 5 mm diameter, a rotation speed of 200 rpm, a rate of penetration of 15 mm/min and a drilling depth of 20 mm. Drilling resistance values per each treatment were calculated as the mean of 6 tests carried out on 2 cubes per each of the nanolimes.

The surfaces of both treated and control samples were observed under a Scanning Electron Microscope in order to evaluate the morphology and distribution within the pores of the calcite crystals originated from the carbonation of nanolime.

Any surface colour variations induced by the nanolime treatments were evaluated with a spectrophotometer (Minolta CM508D Colorimeter) with the CIELab system [43]. 30 measurements were taken in different areas of the surface of each of the treated and control mortar cubes. Total colour variation (ΔE) was calculated by the formula:

$$\Delta E^* = \sqrt{\Delta L^{*2} + \Delta a^{*2} + \Delta b^{*2}}$$

where ΔL^*, Δa^* and Δb^* are the change in luminosity for white-black, red-green and blue-yellow parameters, respectively.

The durability of the treatments was evaluated using a QUV/SE Accelerated Weathering Tester from Q-Lab Europe ltd. Both treated and control mortar cubes were exposed to alternating cycles of UV light and moisture condensation at controlled temperatures in accordance to ASTM G154 CYCLE 4 [44] for a period of 340 h. Each UV cycle has duration of 8 h and uses an irradiance of 1.55 W/m^2 at a temperature of 70 °C. The moisture condensation cycles are carried out at 50 °C with no UV irradiation. The influence of the accelerated weathering on the mortars surface colour and drilling resistance were assessed by colorimetry and DRMS as described above.

3. Results and discussion

3.1. Characterisation of the nanolime suspensions

Fig. 2 shows TEM photomicrographs of the three nanolime products. Hexagonal $Ca(OH)_2$ nanoparticles with identical morphology can be observed in all three of the nanolimes. The crystals tend to agglomerate due to the nanoparticle phenomenon caused by their high surface energy [26,28,31] (Fig. 2a and b). The size of the observed nanoparticles is 250–100 nm for NAN (Fig. 2a), 150–80 nm for CAL (Fig. 2b) and 80–20 nm for LAQ (Fig. 2c). These results are in line with those reported by the developers of the three products [5,17–20,45,46].

The XRD analysis in nitrogen atmosphere (Fig. 3) shows that the only crystalline phase of the three nanolimes is Portlandite ($Ca(OH)_2$, ICSD #01-087-0674), confirming the results of the observations by TEM. For the three samples the strongest peak corresponds to the {0 0 1} basal plane. However, XRD Rietveld refinements showed that LAQ $Ca(OH)_2$ particles have a preferred orientation to the side plane {0 1 0}. NAN and CAL did not show any significant preferred orientation. The Rietveld refinement factors are included in Table 1.

Fig. 4 shows the absorbance (at 600 nm) of NAN, CAL and LAQ dispersions over a period of 2 h following a moderate agitation. A high colloidal stability was observed for NAN and CAL $Ca(OH)_2$ nanoparticles. Previous studies have shown that NAN and CAL nanolimes can keep the colloidal state for more than one week [47]. In contrast, LAQ $Ca(OH)_2$ nanoparticles start to settle about 2 min after agitation (sedimentation rate ≈ 6% per h) and that 12% of the particles settle after 2 h of the testing period. This sedimentation process is considerably slower than that occurring in limewater, where more than 90% of the particles settle in 2 h

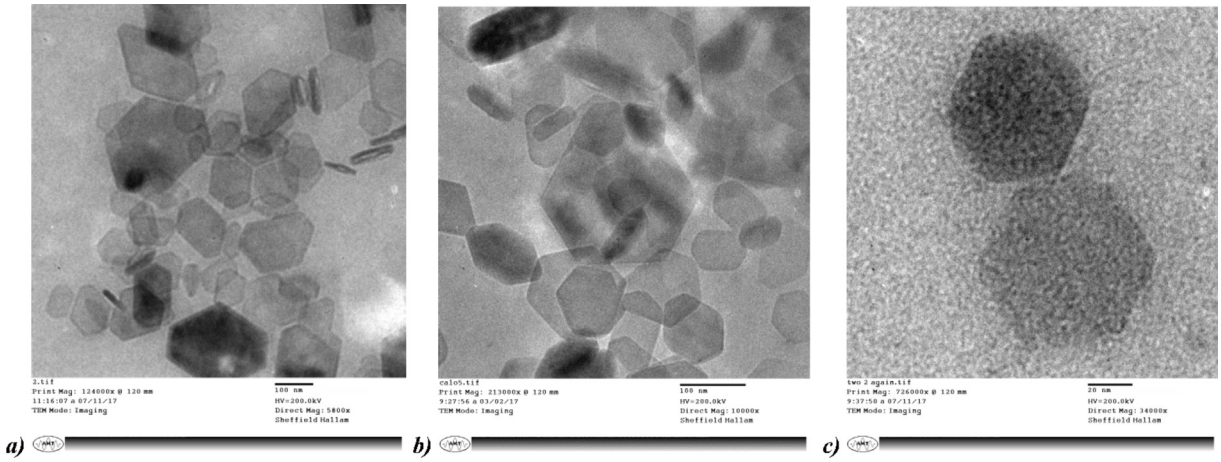

Fig. 2. TEM images of: a) NAN; b) CAL; c) LAQ. Please note that the magnification bar is 100 nm for NAN and CAL, and only 20 nm for LAQ.

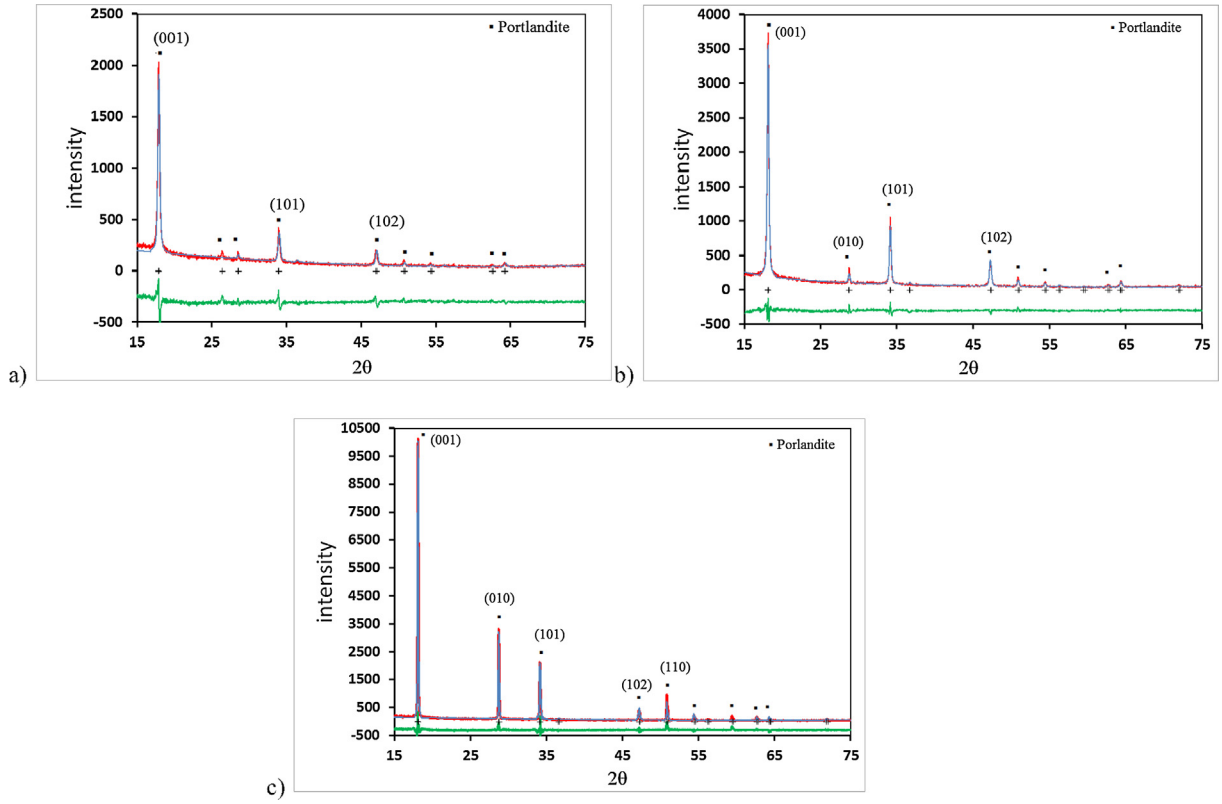

Fig. 3. XRD patterns for NAN (a), CAL (b) and LAQ (c) samples dried in nitrogen atmosphere. Red line corresponds to Intensity observed, blue line to Intensity calculated and green line to the Intensity observed – Intensity calculated difference curve. The crystal phases are shown in brackets and the "+" symbol corresponds to the main peaks.

Table 1
Rietveld refinement factors of samples dried in Nitrogen atmosphere and exposed to air in outdoor conditions (60–80%RH) for 1 h and 7 days.

	Nitrogen			1 h in air			7 days in air		
	NAN	CAL	LAQ	NAN	CAL	LAQ	NAN	CAL	LAQ
R-expected	10.1	9.35	13.89	20.24	20.24	20.03	19.53	15.67	20.03
R-profile	11.69	7.98	11.77	16.13	16.13	15.64	18.52	16.31	15.64
Weighed R profile	14.66	10.38	16.11	20.67	20.67	20.17	24.1	20.81	20.17
Goodness of fit	3.49	1.23	4.34	2.04	2.04	3.01	1.52	1.76	4.31
Phase proportions	100% P	100% P	100% P	90.3% C 9.7% P	100% P	100% C	100% C	75.8%C 24.2% V	100% C
Direction of preferred orientations	NPO	NPO	10	NPO	NPO	NPO	NPO	NPO	104

NPO (No preferred orientation), P (Portlandite); C (Calcite); V (Vaterite).

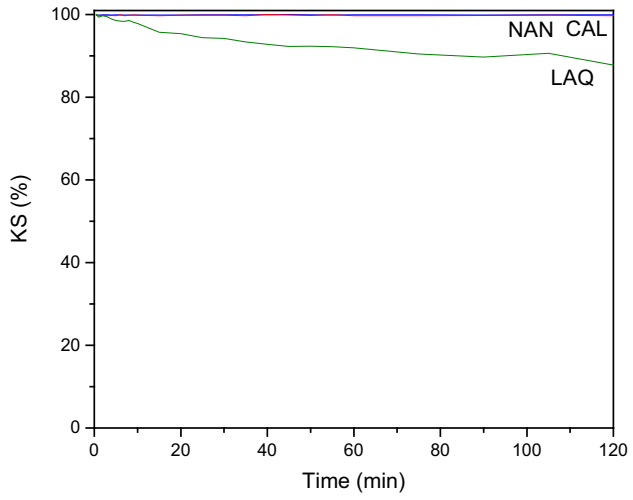

Fig. 4. Kinetic stability KS (%) of NAN, CAL and LAQ dispersions.

[48]. The colloidal stability of LAQ dispersion during the first 2 min after agitation can be considered acceptable for practical purposes as most of the particles remain in colloidal state for the whole length of each application [28]. High colloidal stability is critical to prevent the formation of undesired surface whitening as colloidal particles penetrate better into the pores reducing accumulation on the surface [48].

3.2. Nanolime carbonation process

The XRD patterns of nanolimes exposed to air for 1 h (Fig. 5) show the LAQ nanoparticles to be the most reactive, with calcite (ICSD # 01-085-1108) being the only detected crystalline phase (Fig. 5c). NAN nanoparticles (Fig. 5a) also showed good reactivity within the 1 h of air exposure time, with 90.3% of the sample being composed of calcite (ICSD # 01-072-1652) and 9.7% of portlandite (ICSD # 01-087-0674). The only crystalline phase detected for CAL was portlandite (ICSD # 01-072-0156), indicating a slower carbonation process (Fig. 5b). The relatively high background combined

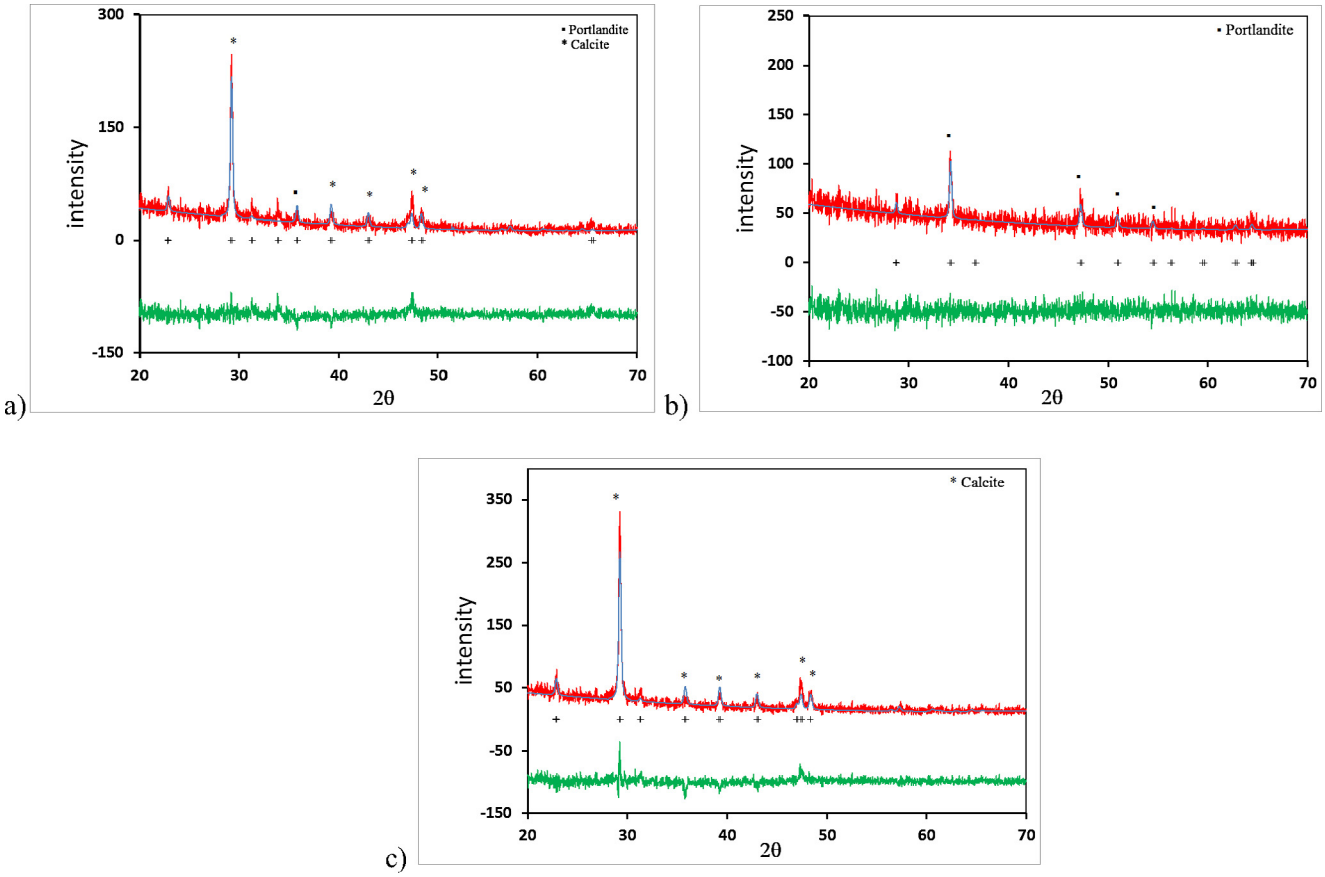

Fig. 5. XRD patterns of NAN (a), CAL (b) and LAQ (c) samples exposed to air in outdoor conditions for 1 h (60–80%RH). Red line corresponds to Intensity observed, blue line to Intensity calculated and green line to the Intensity observed – Intensity calculated difference curve. The crystal phases are shown in brackets and the "+" symbol corresponds to the main peaks.

with broad and weak Bragg peaks recorded for these samples suggest the presence of poorly crystalline phase(s) (Fig. 5).

XRD analysis after 7 days of air exposure shows a better defined crystalline structure for all three samples (Fig. 6) resulting from the completion of the carbonation process. Both NAN and LAQ samples consist entirely of calcite ($CaCO_3$, ICSD# 01-086-2334 and ICSD #01-083-0578 respectively) while CAL is composed of 75.8% of calcite ($CaCO_3$, ICSD# 01-081-2027) and 24.2% of vaterite (ICSD# 01-072-0506). Vaterite is the least stable polymorph of calcium carbonate, calcite being the most stable one [29,30]. In previous studies [24], Calosil was found to precipitate as calcite and aragonite. XRD-Rietveld shows the calcite crystals in LAQ (Fig. 6c) are fully oriented to {1 0 4} while the crystals in NAN and CAL have no preferred orientation. The Rietveld refinement factors are included in Table 1.

TEM images taken after 1 min of air exposure show that during the carbonation process NAN and CAL tend to grow mainly as hexagonal plates (Fig. 7a, b) while LAQ nanoparticles can be seen to grow preferentially through the {0 1 0} side plane (Fig. 7c). SEM images taken after 7 days exposure to outdoor conditions show NAN and CAL being characterised by calcium carbonate crystals of irregular shape (Fig. 7d–e), while LAQ shows calcite in well-formed hexagonal prisms and parallelepiped shapes (Fig. 7f), presenting larger size (10 μm) than NAN and CAL ones, despite the smaller original nanoparticle size. Prismatic calcite crystals with similar shape to that observed for LAQ have been described by Ukrainczyk et al [49] when examining the influence of additives on the growth of calcite crystals.

3.3. Effectiveness of the nanolime treatments

The pore structure properties of treated and control mortars are summarised in Table 2. It is evident that all three treatments affect the pore structure of the mortar by reducing the modal pore diameter and the porosity while increasing the total pore surface area. The highest porosity decrease was observed for the mortar treated with NAN (26% decrease), followed by those treated with LAQ (21%) and CAL (16%). The pore size distributions of control and treated mortars are shown in Fig. 8. It can be seen that the control sample has a tri-modal pore size distribution, coarser pores with diameters between 25 μm and 100 μm, intermediate pores with diameters between 3 μm and 25 μm and finer pores with diameters between 0.06 μm and 0.7 μm. Following the treatments, a complete removal of the coarsest mode and enhancement of the intermediate mode can be observed (Fig. 8). Such enhancement is more prominent for the mortar treated with CAL (Fig. 8), which is in line with the lower decrease in porosity observed for this mortar.

The water absorption and drying curves are reported in Fig. 9. Apparent porosity by immersion, water absorption and drying characteristics are reported in Table 3.

Capillary rise in a porous material is strongly influenced by pore size distribution. The pore diameter range affecting water capillary rise and transport could theoretically be considered to range between 1 mm and 1 μm diameter [50]. It is shown that all three treatments yield a decrease of the capillary water absorption coefficient of the mortar. This decrease can be attributed to the reduc-

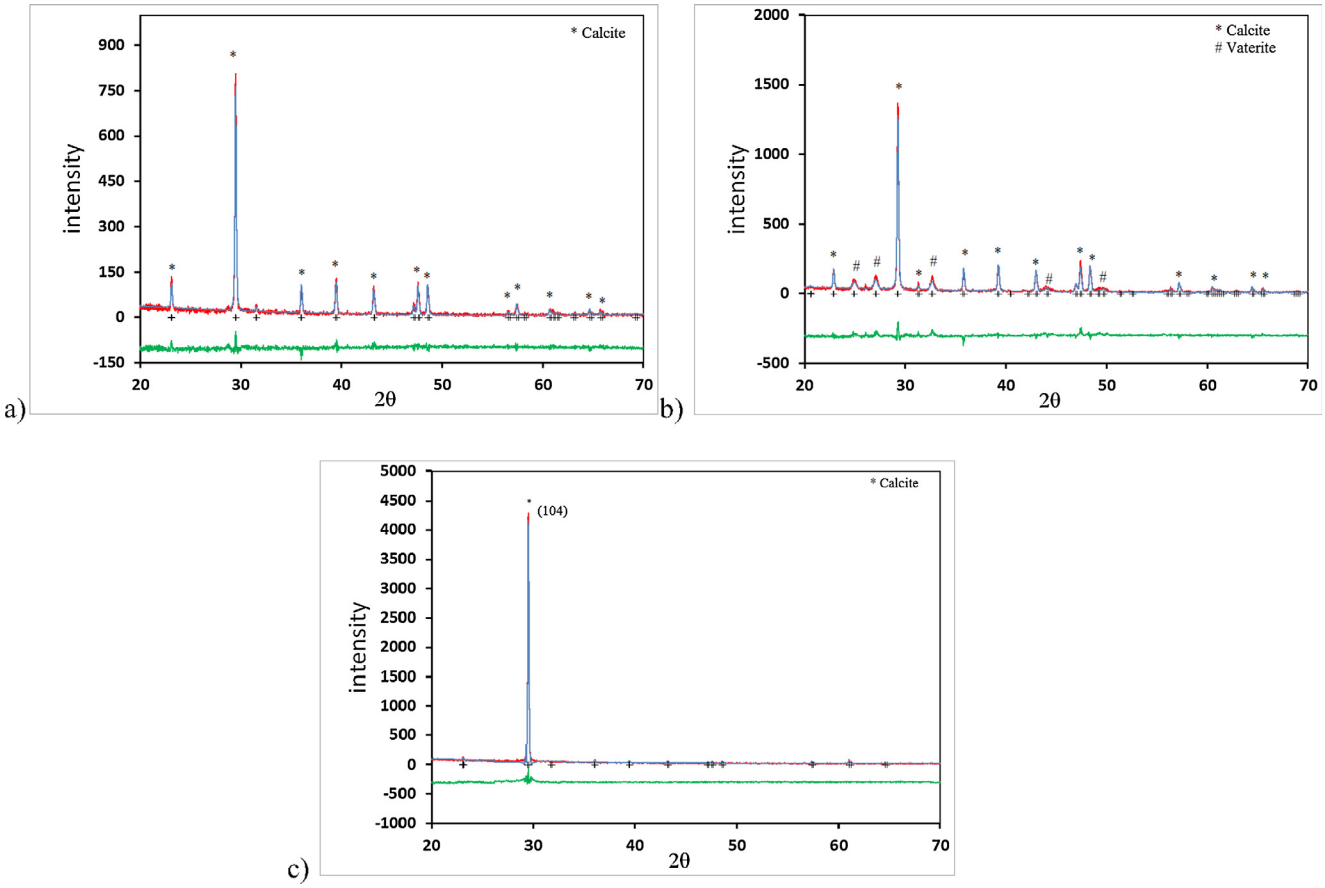

Fig. 6. XRD patterns of NAN (a), CAL (b) and LAQ (c) samples exposed to air in outdoor conditions for 7 days (60–80%RH). Red line corresponds to Intensity observed, blue line to Intensity calculated and green line to the Intensity observed – Intensity calculated difference curve. The crystal phases are shown in brackets and the "+" symbol corresponds to the main peaks.

tion in the number of pores with diameters between 17 μm and 100 μm, which results from the applied treatments and was also recorded by the MIP measurements. Fig. 9a and Table 3 show that the NAN treatment yielded the biggest decrease in WAC (42%), followed by CAL (14%) and LAQ (4%). Control samples required about 7 h of contact with water to reach asymptotic values while treated samples took nearly 9 h (Fig. 9a). The latter absorbed less water by both capillarity and 24-hour immersion, with the NAN treated sample showing the greatest decreases.

The treatments also reduced the apparent porosity of the mortar, with the NAN treated samples showing the highest reduction (11.4%) followed by LAQ (5.7%) and CAL (2.1%). These results are fully compatible with the results of the porosity measurements by MIP reported above. The average apparent porosity of the treated samples show a relatively high standard deviation reflecting the inhomogeneity of the applied treatment, with the CAL (±0.40) being only twice the value of the control, while LAQ (±0.65) is thrice higher than the control and NAN (±1.63) being significantly higher (Table 3).

The drying curves (Fig. 9b) and the measured initial and final drying rates (Table 3) show that treated mortar samples take far more time to dry than the control ones. This is an undesirable behaviour as it increases the risk of spalling when the mortar is exposed to freeze-thaw cycles (limited to the external 1 cm plus where the nanolime precipitates) and/or biological attack [51]. The drying rate reduction is attributed to the finer pore structure of the mortar near the surface of the sample which results from the nanolime treatment. The smaller pores in the denser mortar layer reduce the liquid water transport towards the surface hence slowing down the drying kinetics [51]. The lowest initial drying rate was observed for the mortar treated with CAL while NAN and LAQ yielded similar rates. Whilst control samples were completely dry after 50 h, treated samples still contained some residual moisture after 72 h (Table 3).

Table 4 shows the results of the Scotch Tape Test (STT). A significant decrease of removed material ($\Delta V \approx 90\%$) was observed for all treated mortars with no significant differences in the performance of the three nanolimes. The standard deviation of the ΔV (%) (SD) shown in the table confirms a good reliability for this test in the measuring of surface cohesion.

Drilling resistance results are shown in Fig. 10. It can be seen that whilst the control sample shows a steady drilling resistance throughout the drilling depth (average force ≈ 0.07 N), the treated samples show increased resistance within the first 10 mm from the surface. The highest average drilling resistance was observed for the mortar treated with NAN (average force ≈ 0.57), followed by those treated with CAL (average force ≈ 0.32) and LAQ (average force ≈ 0.27). This is fully compatible with the porosity results which showed a more marked decrease of porosity for NAN treated samples than for CAL and LAQ treated samples. The average drilling resistance in the outer 5 mm is 0.09 N for Control, 1.12 N for NAN, 0.68 N for CAL and 0.64 N for LAQ, which is also in line with the results of the MIP measurements. This trend was not observed in the results of the Scotch Tape Test, possibly due to a lower sensitivity of this technique compared to that of the DRMS. The DRMS profiles in Fig. 10a-c show that the drilling resistance of the treated

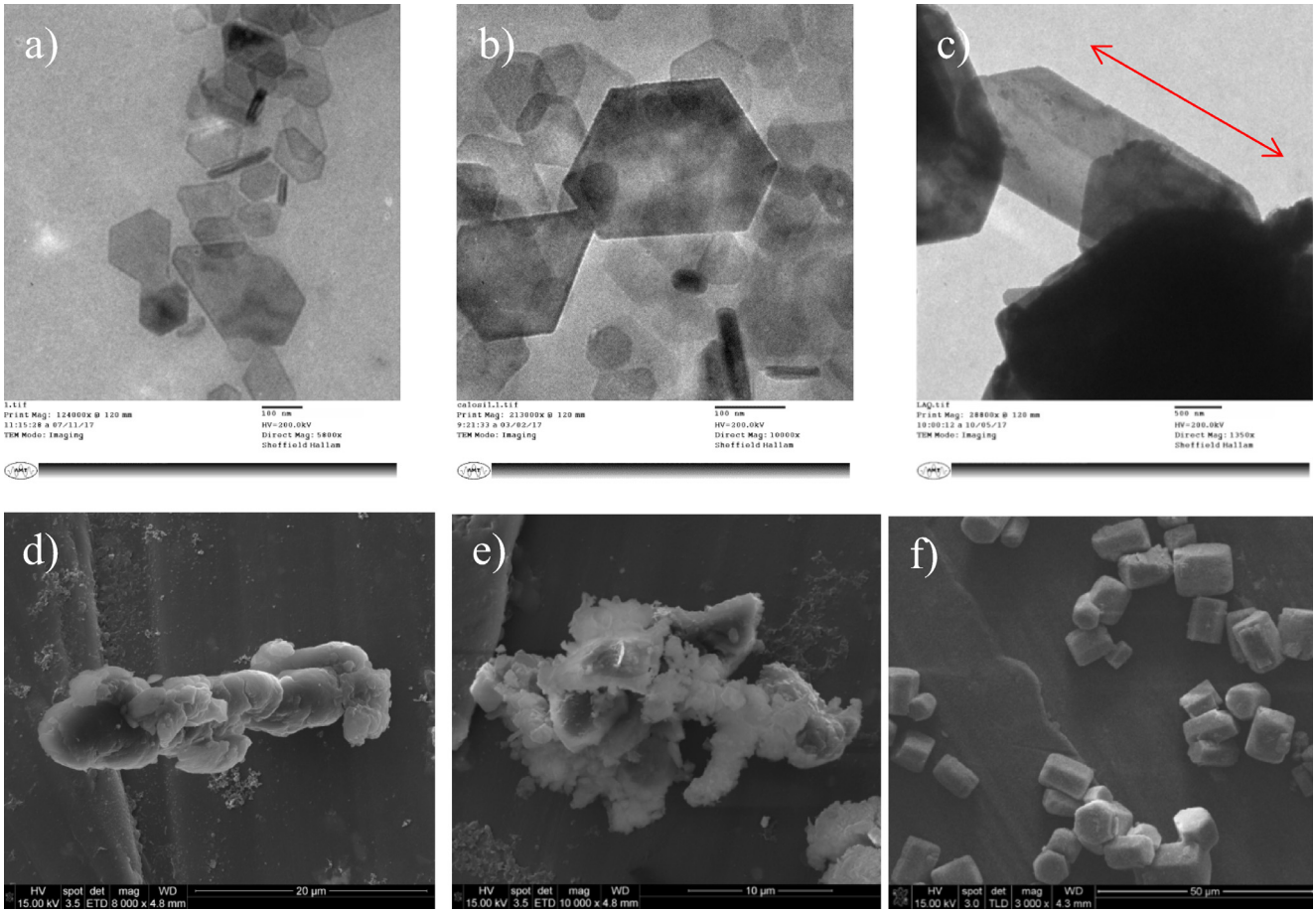

Fig. 7. a) TEM image of NAN after 1 min of air exposure at 124,000×; b) TEM image of CAL after 1 min of air exposure at 213,000×; c) TEM image of LAQ after 1 min of air exposure at 28,800×; d) SEM image of NAN after 7 days at 8,000×; e) SEM image of CAL after 7 days at 10,000×; f) SEM image of LAQ after 7 days at 3,000×.

Table 2
Pore structure properties of treated and control mortar samples measured by MIP.

Sample	Porosity (%)	Modal pore diameter (μm)	Total pore surface area (m^2/g)
Control	22.63	18.09	0.45
NAN	16.75	15.23	0.575
CAL	18.92	13.55	0.585
LAQ	17.87	14.15	0.781

samples decreases with depth until it reaches the resistance of the control sample at about 10 mm for NAN and CAL and about 6 mm for LAQ. This data seems to indicate for the NAN and CAL treatments a deeper penetration into the mortar compared to the LAQ treatment.

The drilling resistance tests were repeated after exposing the samples to alternating cycles of UV light and moisture (Fig. 10d-f) and the results show for the NAN and CAL treated samples a reduction of the depth at which the drilling resistance reaches that of the control samples. This could indicate that a certain amount of material got partially dissolved from the surface of these samples as a result of the exposure to the alternating cycles of UV light and moisture condensation at elevated temperatures in the tester. The presence of deposits of white powder material in the water pan just below the sample holder panel seems to support this interpretation. The DRMS profile of the LAQ treated sample is similar to that recorded before the accelerated weathering test (Fig. 10f), which seems to indicate that less or no material loss occurred on the surface of this sample. The apparent higher resistance to weathering of the LAQ treated sample compared to that of the NAN and CAL treated ones could be attributed to a better developed crystalline structure and larger crystals. As described in Section 3.2, LAQ produces perfectly shaped prismatic and parallelepiped calcite crystals of a larger size compared to NAN and CAL, which present poorly crystallized ones. The "well-shaped" calcite crystals are more resistant to dissolution than irregular shaped crystals as is well known [52]. In the case of the CAL treated sample, a reduction of the drilling resistance was observed within the first millimeter of depth (Fig. 10e), which could be due to the solubility of metastable amorphous carbonate phases such as vaterite (see Section 3.2).

Both treated and untreated mortar surfaces were observed by SEM in order to study the distribution of the nanolime in the pores and the morphology of the calcite crystals. SEM micrographs showed for the control samples a great number of large pores (pore diameter > 100 μm), which are outside of the measurement range of the used MIP technique (Fig. 11a). Following the treatments, the reduction of porosity and pore size due to the deposition of calcite inside the pores is clearly visible (Fig. 11b-d).

In Fig. 11b-d it can be seen that the nanolime is distributed homogeneously in the pores of the mortar and seems to adhere well to the substrate to the point that it is not easy to distinguish between the mortar and the newly precipitated calcite which fills the pores reducing their size. Fig. 12a shows that the calcitic

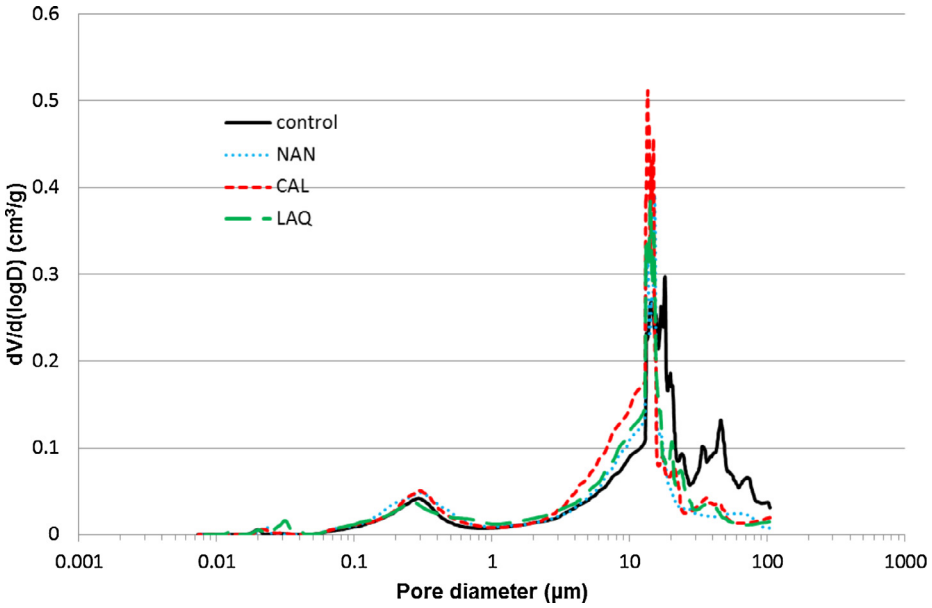

Fig. 8. Differential volume of intruded mercury versus pore diameter of treated and control mortar samples.

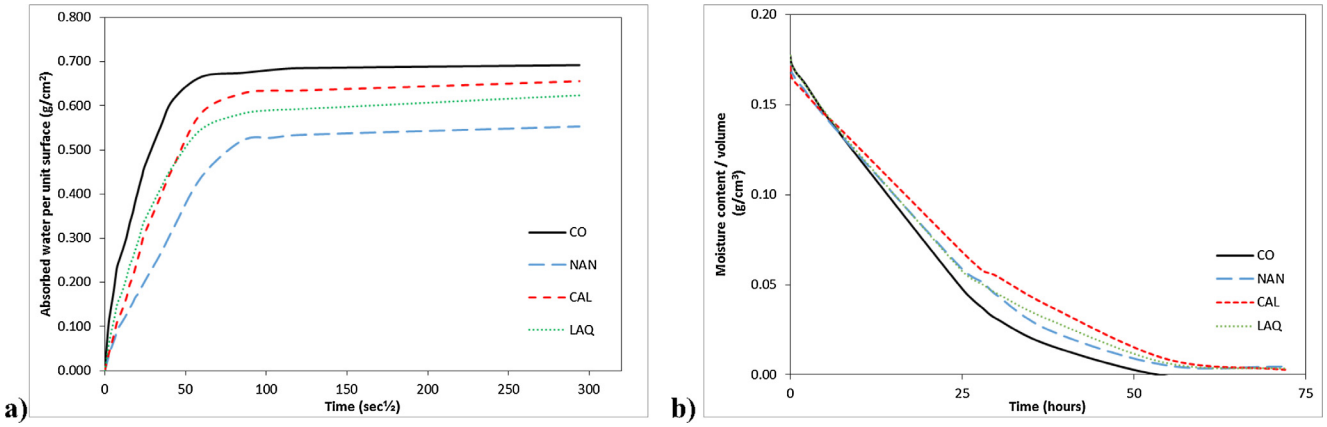

Fig. 9. Capillary absorption (a) and drying curves (b) for control and NAN, CAL and LAQ treated mortars.

Table 3
Apparent porosity by immersion, capillary water absorption and drying characteristics.

Parameter	CO	NAN	CAL	LAQ
Apparent porosity (%)	11.84 (±0.20)	10.49 (±1.63)	11.60 (±0.40)	11.17 (±0.65)
Water absorption coefficient (10^{-3} g/cm^2 s$^{0.5}$)	9.5 (±0.78)	5.5 (±1.7)	8.2 (±2.5)	9.1 (±0.5)
Water absorbed at asymptotic value (g)	11.00 (±0.06)	8.95 (±1.05)	10.60 (±0.52)	10.32 (±0.68)
Water absorbed after 24-hour immersion (g)	11.57 (±0.16)	10.34 (±1.61)	11.49 (±0.38)	11.07 (±0.50)
Initial drying rate (10^{-3} g/cm^3 h)	4.9 (±0.1)	3.9 (±0.3)	4.4 (±0.5)	4.4 (±0.3)
Final drying rate (10^{-3} g/cm^3 h)	1.0 (±0.3)	1.0 (±1.0)	1.2 (±0.6)	1.2 (±0.5)
Moisture content after 72 h (g/cm^3)	0.01 (±0.01)	1.81 (±0.01)	1.94 (±0.02)	2.02 (±0.02)
Time for total drying (h)	±50	>72	>72	>72

Values in parentheses are standard deviation of the three cubic samples.

material resulting from the carbonation of NAN within the mortar presents a different variety of shapes (mostly rhombohedral with scalenohedral terminations), which were observed also in previous studies for the same nanolime [24]. CAL precipitated in the form of calcite rhombohedra and some vaterite (Fig. 12b). Fig. 12c shows typical calcite prisms on the LAQ sample. These are larger than those formed by NAN and CAL hence resulting in a smaller specific surface which is associated with higher resistance to weathering [52]. This morphology is similar to that visible on the SEM images (Section 3.2).

Table 4
Scotch tape test results. Values determined on 9 measurements.

Treatment	Removed material (mg/cm^2)		ΔV (%)	SD
	Before treatment	After treatment		
NAN	26.85 (±1.24)	2.54 (±3.96)	90.54	5.1
CAL	26.71 (±1.56)	1.71 (±0.73)	93.60	2.3
LAQ	26.76 (±1.04)	3.16 (±2.57)	88.19	3.6

Scotch area: 3 × 1.5 cm; Values in parentheses are standard deviation for the nine measurements taken on each of the three cub samples.

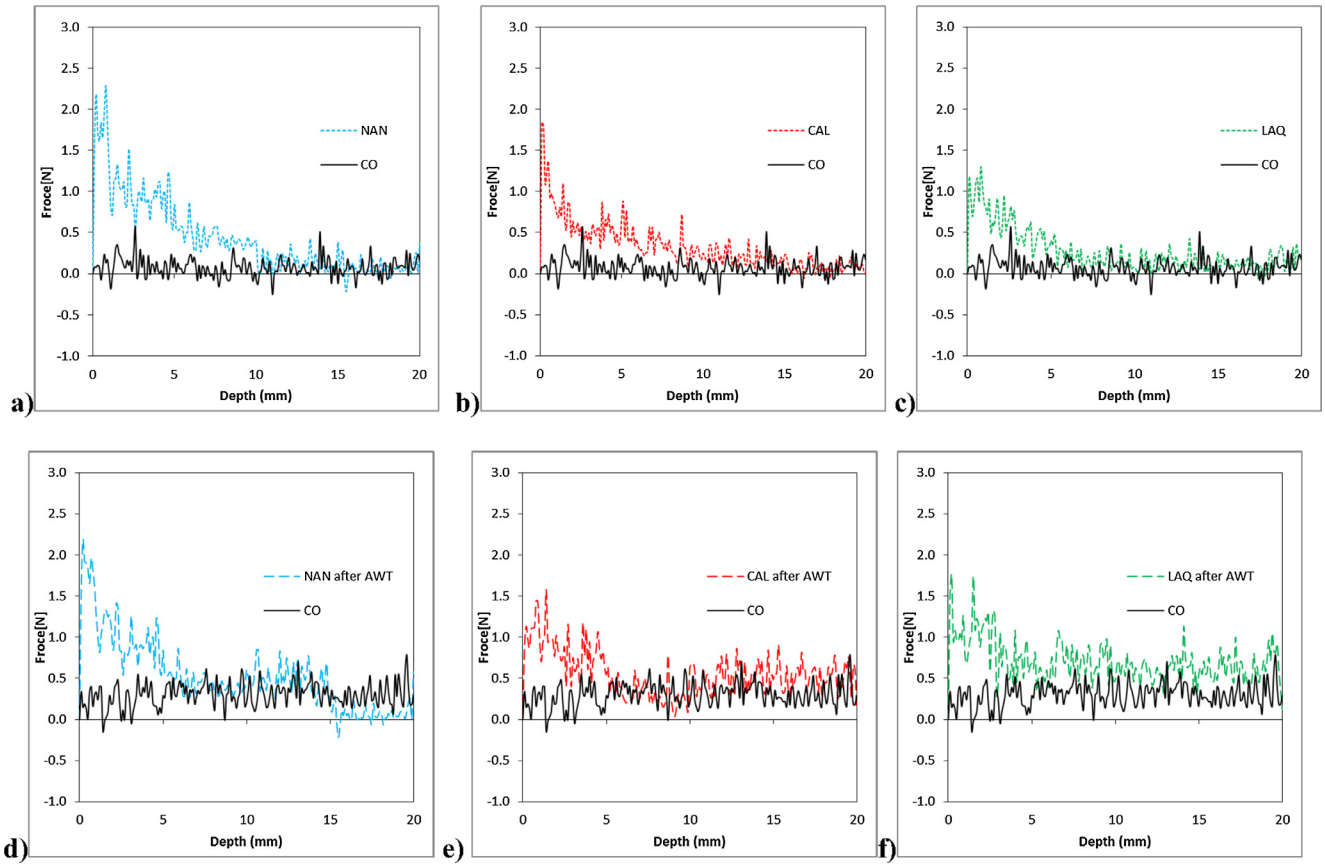

Fig. 10. Drilling resistance of: a) NAN; b) CAL; c) LAQ; d) NAN after AWT; e) CAL after AWT and f) LAQ after AWT.

Ideally consolidation treatments should improve the physical-mechanical properties of the treated material without affecting its aesthetic appearance. However, a common side effect of the use of nanolime is a whitening of the surface following treatment. In order to investigate the occurrence of this phenomenon in association with the use of the tested nanolimes, spectrophotometric analyses were carried out to measure changes in L^* (white-black parameter) and ΔE^* (total colour variations) following treatment. ΔE^* values <5 are considered suitable for practical conservation interventions and visually imperceptible [28]. The results (Table 5) show that all of the three treatments cause whitening of the surface with both ΔE^* and ΔL^* values above 5. NAN yielded the lowest whitening effect ($\Delta L^* \approx 6$ and total colour alteration $\Delta E^* \approx 6$). CAL and LAQ caused a more significant whitening effect with $\Delta L^* \approx 7.5$ and $\Delta L^* \approx 11.94$, respectively, and total colour change with $\Delta E^* \approx 9$ and $\Delta E^* \approx 14$, respectively. In previous studies, NAN and CAL yielded chromatic alterations of about $\Delta E^* \approx 6$ and $\Delta E^* \approx 4$, respectively [24]. The lower colloidal stability of LAQ is considered responsible for the more significant formation of undesired surface whitening. Nonetheless, the observed whitening and total chromatic alterations are still lower than those caused by the lime-water technique, which normally vary between $\Delta L^* \approx 50$ to 70 [9,25].

The whitening effect and total colour changes associated with the application of nanolime decreased after the samples were exposed to UV light and moisture cycles in the accelerated weathering test, with both ΔE^* and ΔL^* decreasing below 5. This could indicate that the induced weathering dissolved a certain amount of material from the surface of the samples, as also detected by the DRMS for the NAN and CAL samples. It is apparent that in the case of the LAQ samples the amount of material that got dissolved from their surface during the accelerated weathering test was sufficient to reduce the whitening but too small to be detected by the DRMS.

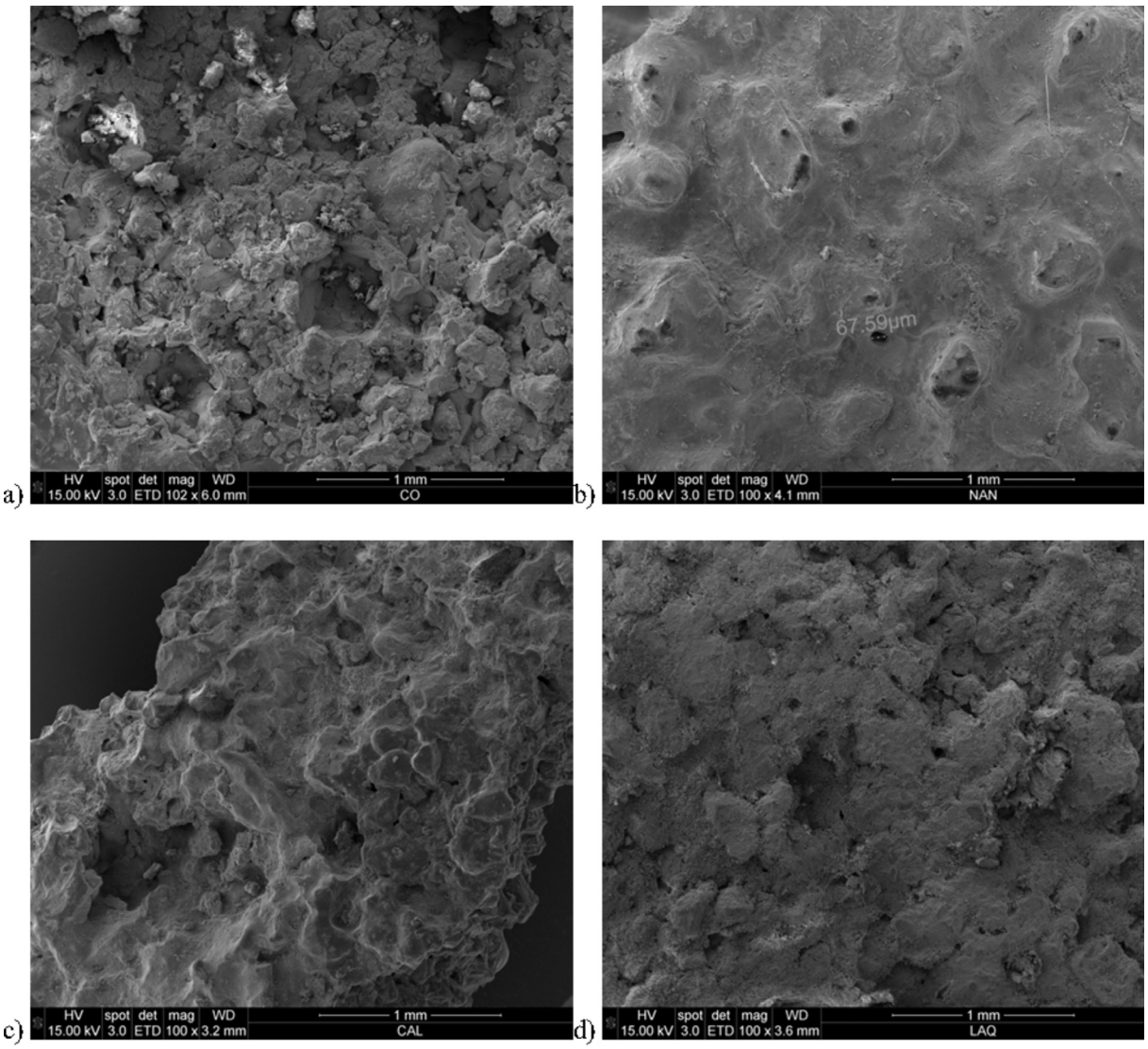

Fig. 11. SEM micrographs of mortar samples (100 X): a) control sample; b) surface treated with NAN; c) surface treated with CAL; d) surface treated with LAQ.

4. Conclusions

This study has shown that NAN, CAL and LAQ can be used effectively for the consolidation of highly porous calcareous materials such as lime mortars and represent a viable alternative to organic consolidants for their consolidation. It has been proven that repeated applications of low concentration dispersions of these nanolimes can restore the substrate superficial cohesion, improve its mechanical properties, reduce its porosity, number of micropores (10–100 μm) and water absorption coefficient.

It has been shown that:

- The $Ca(OH)_2$ nanoparticles of the three nanolimes consist of crystalline hexagonal plates with similar shapes. However, there is a difference in size: LAQ nanoparticles are smaller than both NAN and CAL. XRD-Rietveld refinements showed that LAQ $Ca(OH)_2$ particles tend to align in a preferential direction along the side plane {0 1 0} whereas NAN and CAL did not show any significant preferred orientation. Nanorestore Plus® and Calosil® are stable colloidal dispersions while LAQ nanoparticles start to settle about 2 min after agitation (sedimentation rate $\approx$ 6% per h) and the 12% of the particles has settled after 2 h. This sedimentation rate is considered acceptable for practical purposes as most of the particles remain in colloidal state during the time of the application. However, a moderate agitation is highly recommended before the application of this nanolime. Moreover, the application should ideally be completed within the first 2 first minutes after the agitation, before the particles start to settle.
- Nanolime particles created by anion exchange synthesis (LAQ) are the most reactive with calcite being the only detected crystalline phase after 1 h of air exposure. NAN particles also showed a good reactivity with 90% of the sample being composed of calcite following the same exposure time. CAL particles showed slower carbonation and no calcite had formed after 1 h exposure. After 7 days both LAQ and NAN consisted entirely of calcite, while CAL was composed approximately of 75% of calcite and 25% of vaterite, which is a metastable phase of calcium carbonate, less stable than calcite.
- During the carbonation process, NAN and CAL tend to grow mainly as hexagonal plates while LAQ nanoparticles seem to grow preferentially through the {0 1 0} side plane. After 7 days

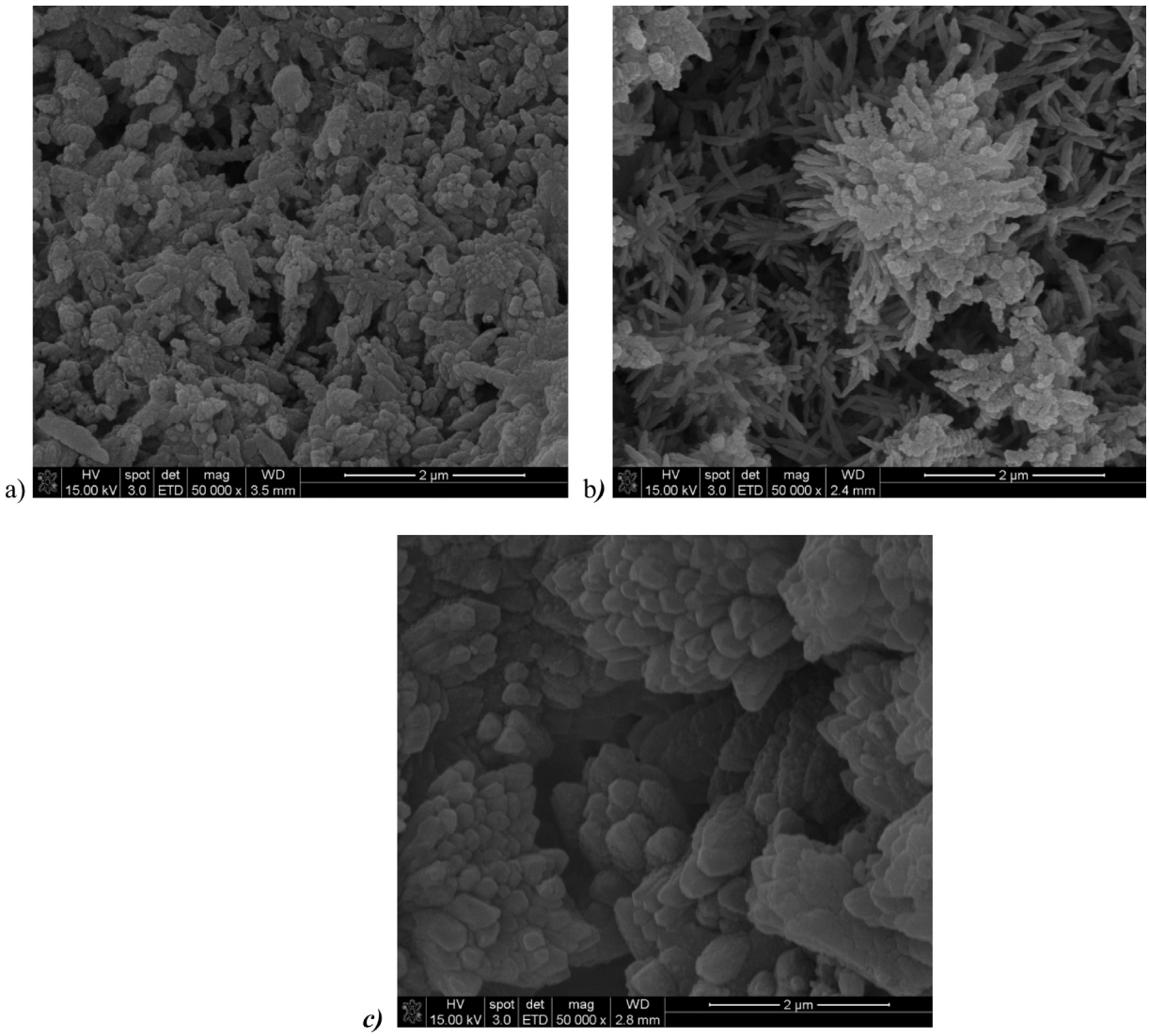

Fig. 12. SEM detail micrographs of carbonated nanolime: a) NAN 50,000×; b) CAL 50,000×; c) LAQ 50,000×.

Table 5
Chromatic alterations of treated samples before and after the Accelerated Weathering Test.

	ΔL^*		Δa^*		Δb^*		ΔE^*	
	Treated	AWT	Treated	AWT	Treated	AWT	Treated	AWT
NAN	6.33 (±0.20)	3.18 (±0.43)	−1.48 (±0.16)	−0.48 (±0.20)	−0.43 (±0.91)	−1.96 (±0.55)	6.51	3.76
CAL	7.50 (±0.51)	2.53 (±0.90)	−0.75 (±0.13)	−0.37 (±0.16)	−4.64 (±0.69)	−0.88 (±1.15)	8.85	2.7
LAQ	11.94 (±0.96)	4.04 (±0.63)	−1.25 (±0.15)	−0.55 (±0.0.26)	−6.96 (±1.07)	−1.17 (±1.45)	13.87	4.24

Values determined on 30 measurements; AWT (Accelerated Weathering Test).

of carbonation, LAQ shows well-formed hexagonal calcite prismatic crystals with larger size than NAN and CAL, which consist of calcite crystals of irregular shape. XRD-Rietveld shows the calcite crystals in LAQ are fully oriented to {1 0 4} while the crystals in NAN and CAL have no preferred orientation.

- All treatments affect the pore structure by reducing the porosity of the superficial portion of the mortar. The reduction in porosity is attributed mainly to a reduction of the number of pores with diameter between 17 μm and 100 μm, which also decreases the capillary water absorption coefficient. Nanorestore Plus® presented the highest reduction of the porosity and water absorption by capillarity rate.
- All three nanolimes increase the drilling resistance of the mortar surface. The penetration depth of nanolime appears to be approximately 1 cm for NAN and CAL and 0.6 cm for LAQ. NAN treated mortars showed the highest increase in drilling resistance, which is in line with their highest reduction in porosity; followed by those treated with CAL and LAQ. Following an accelerated weathering test, the DRMS detected the loss of a certain amount of material from the surface of mortars treated with NAN and CAL. This was not observed for LAQ treated samples, possibly due to LAQ better developed crystalline structure providing higher resistance to dissolution processes during the accelerated weathering test. The detected loss is slightly

more pronounced in Calosil® samples, possibly as a consequence of the dissolution of metastable vaterite. A study of the calcite morphology and structural features of LAQ nanolime must be addressed in future studies to better understand the performance of this nanolime.

- Following treatment, the samples take far more time to dry due to a finer pore structure of the mortar near the surface. This is an undesirable behaviour which may lead to deterioration processes. Specifically, spalling can occur where moisture is present and the mortar is exposed to freeze-thaw cycles. Furthermore, longer drying times can favour biological growth and the dissolution of poorly crystallised calcite and vaterite. A full study of the durability of mortars treated with the three nanolimes will be carried out in future research.
- All treatments produced an undesired whitening of the surface after application. LAQ treatment induced the highest whitening effect which can be attributed to the lower colloidal stability of this nanolime. The whitening effect associated with all treatments decreases to values which are imperceptible to the naked eye after exposing the samples to the Accelerated Weathering Test. This could indicate that a superficial layer of the consolidated mortar was partially dissolved during the accelerated weathering test, as also observed by DRMS. In the case of LAQ treated mortars the dissolution decreased the whitening without causing significant thickness reduction.

One final conclusion of this study is that substrates treated with the studied nanolimes will require regular maintenance (i.e. periodic application of nanolime) in order to achieve long term performance in terms of mechanical and physical properties. Further work carried out by the authors has focused on the influence of the use of different types of solvents on the performance of LAQ nanolime and a report will be submitted for publication in due course.

5. Declaration of conflicting interests

The authors declare that there is no conflict of interest and take a neutral position to offer an objective evaluation of the consolidation process.

Acknowledgements

This research has been funded by a Vice Chancellor's Scholarship within the Doctorate Program at Sheffield Hallam University (UK). The authors want to thank Dr. Anthony Bell for his support with Rietveld refinements.

References

[1] E. Doehne, C.A. Price, in: Stone Conservation: An Overview of Current Research, 2nd edition., Research in Conservation, the Getty Conservation Institute, Getty Publications, Los Angeles, 2011, pp. 35–37.
[2] A.E. Charola, R. Ware, Acid deposition and the deterioration of stone: a brief review of a broad topic, in: G.S. Siegesmund, A. Vollbrecht, T. Weiss (Eds.), Natural stone, weathering phenomena, conservation strategies and case studies, Special Pu (London), 2002, pp. 393–406. Available at: doi:10.1144/GSL.SP.2002.205.01.28.
[3] E. Hansen, E. Doehne, J. Fidler, et al., A review of selected inorganic consolidants and protective treatments for porous calcareous materials, Rev. Conserv. 4 (2013) 3630.
[4] M.E. Young, M. Murray, P. Cordiner, Stone consolidants and chemical treatments in Scotland. Report to Historic Scotland, 1999.
[5] M. Ambrosi, L. Dei, R. Giorgi, et al., Colloidal particles of $Ca(OH)_2$: properties and applications to restoration of frescoes, Langmuir 17 (14) (2001) 4251–4255. Available at: ttp://pubs.acs.org/doi/abs/10.1021/la010269b.
[6] F. Henriques, A.E. Charola, A comparative study of standard test procedures for mortars, in: Proceddings of the 8th International Congress on Deterioration and Conservation of Stone, (1996) 1521–1528.
[7] C. Price, K. Ross, G. White, A further appraisal of the 'Lime Technique' for limestone consolidation, using a radioactive tracer, IIC J. Stud. Conserv. 33 (4) (1988) 178–186.
[8] I. Brajer, N. Kalsbeek, Limewater absorption and calcite crystal formation on a limewater-impregnated secco wall-painting, Stud. Conserv. 44 (3) (1999) 145–156.
[9] Z. Slizkova, M. Dracky, A. Viani, Consolidation of weak mortars by means of saturated solution of calcium hydroxide or barium hydroxide, J. Cult. Heritage 16 (4) (2015) 420–460.
[10] S. Bracci, B. Sacchi, A.F. Pinto, et al., Inorganic consolidants on stone artifacts: optimization of application procedures for marble and limestones". International Symposium "Stone consolidation in cultural heritage: research and practice", Lisbon 6-7 May, 2008. Proceedings, in: J. Delgado Rodrigues & João Manuel Mimoso (Eds.), (2008) 81–90.
[11] G. Wheeler, in: Alkoxysilanes and Consolidation of Stone, The Getty Conservation Institute, Getty Publications, Research in Conservation, Los Angeles, 2005, pp. 31–48.
[12] A.E. Charola, A. Tucci, On the reversibility of treatments with acrilic/silicone resin mistures, J. Am. Inst. Conserv. 25 (1986) 83–92.
[13] A.E. Charola, Water-repellent treatments for building stones: a practical overview Available at:, Assoc. Preserv. Technol. Int. (APT) 26 (2) (1995) 10–17. http://www.jstor.org/stable/1504480.
[14] F. Jroundi, A. Fernández-Vivas, C. Rodriguez-Navarro, et al., Bioconservation of deteriorated monumental calcarenite stone and identification of bacteria with carbonatogenic activity, Microb. Ecol. 60 (2010) 39–54.
[15] P. Baglioni, R. Carrasco-Vargas, D. Chelazzi, et al., The maya site of Calakmul: in situ preservation of wall painting and limestone using nanotechnology, Stud. Conserv. 51 (2) (2006) 162–169, https://doi.org/10.1179/sic.2006.51.Supplement-2.162.
[16] J. Otero, A.E. Charola, C. Grissom, et al., An overview of nanolime as a consolidation method for calcareous substrates, Ge-Conservación J. 11 (1) (2017) 71–78, https://doi.org/10.17265/2162-5298.
[17] G. Taglieri, V. Daniele, L. Macera, et al., Nano $Ca(OH)_2$ synthesis using a cost-effective and innovative method: Reactivity study, J. Am. Ceram. Soc. 100 (2017) 5766–5778.
[18] G. Taglieri, B. Felice, V. Daniele, et al., Analysis of the carbonatation process of nanosized $Ca(OH)_2$ particles synthesized by exchange ion process, Proc. Inst. Mech. Eng., Part N: J. Nanoeng. Nanosystems 230 (1) (2016) 25–31.
[19] R. Volpe, G. Taglieri, V. Daniele, et al., A process for the synthesis of $Ca(OH)_2$ nanoparticles by means of ionic exchange resin, European patent EP2880101 (2016).
[20] P. Baglioni, D. Chelazzi, R. Giorgi, et al., Commercial $Ca(OH)_2$ nanoparticles for the consolidation of immovable works of art, Appl. Phys. A 114 (2014) 723–732.
[21] D. Costa, Rodrigues J. Delgado, Consolidation of a porous limestone with nanolime, in: Proceeding of 12th International Congress on Deterioration and Conservation of Stone, Columbia University, New York, 2012, pp. 22–26.
[22] A. Campbell, A. Hamilton, T. Stratford, et al., Calcium hydroxide nanoparticles for limestone conservation: imbibition and adhesion, in: Proceedings of Symposium Adhesive and Consolidants for Conservation: Research and Applications, ICC, Ottawa, 2011, pp. 17–21.
[23] E. Ghaffari, T. Koberle, J. Weber, Methods of polarising microscopy and SEM to assess the performance of nanolime consolidants in porous solids, in: Proceeding of 12th International Congress on Deterioration and Conservation of Stone, Columbia University, New York, 2012, pp. 22–26.
[24] A. Arizzi, L.S. Gomez-Villalba, P. Lopez-Arce, et al., Lime mortar consolidation with nanostructured calcium hydroxide dispersions: the efficacy of different consolidating products for heritage conservation, Eur. J. Mineral. 27 (3) (2013) 311–323.
[25] Z. Slizkova, D. Frankeová, Consolidation of a porous limestone with nanolime, in: Proceedings of the 12th International Congress on the Deterioration and Conservation of Stone, New York, 2012.
[26] G. Borsoi, B. Lubelli, R. Van Hees, et al., Understanding the transport of nanolime consolidants within Maastricht limestone, J. Cult. Heritage 18 (2016). 242 24.
[27] S.A. Ruffolo, M.F. La Russa, P. Aloise, et al., Efficacy of nanolime in restoration procedures of salt weathered limestone rock, Appl. Phys. A Mater. Sci. Process. 114 (2014) 753–758.
[28] C. Rodriguez-Navarro, A. Suzuki, E. Ruiz-Agudo, Alcohol dispersions of calcium hydroxide nanoparticles for stone conservation, Langmuir 29 (2013) 11457–11470.
[29] P. López-Arce, L.S. Gomez-Villalba, L. Pinho, et al., Influence of porosity and relative humidity on consolidation of dolostone with calcium hydroxide nanoparticles: effectiveness assessment with non-destructive techniques, Mater. Charact. J. 61 (2010) 168–184, https://doi.org/10.1016/j.matchar.2009.11.007.
[30] P. Lopez-Arce, L.S. Gomez-Villalba, Martinez-Ramirez,, et al., Influence of relative humidity on the carbonation of calcium hydroxide nanoparticles and the formation of calcium carbonate polymorphs, Powder Technol. 205 (2011) 263–269, https://doi.org/10.1016/j.powtec.2010.09.026.
[31] C. Rodriguez-Navarro, I. Vettori, E. Ruiz-Agudo, Kinetics and mechanism of calcium hydroxide conversion into calcium alkoxides: implications in heritage conservation using nanolimes, Lagmuir (2016), https://doi.org/10.1021/acs.langmuir.6b01065.

[32] G. Taglieri, J. Otero, V. Daniele, et al., The biocalcarenite stone of Agrigento (Italy): Preliminary investigations of compatible nanolime treatments, J. Cult. Heritage (2017), https://doi.org/10.1016/j.culher.2017.11.003.
[33] The European Standard EN 1015-3:1990, (1990), Methods of test for mortar for masonry. Determination of consistence of fresh mortar (by flow table).
[34] The European Standard EN 1015-2:1998, (1998), Methods of test for mortar for masonry. Bulk sampling of mortars and preparation of test mortars.
[35] H.M. Rietveld, A profile refinement method for nuclear and magnetic structures, J. Appl. Crystallogr. 10 (1969) 65.
[36] D.L. Bish, J.E. Post, Modern Powder Diffraction, Mineralogical Society of America, Washington, 1989.
[37] The English Standard EN 13755 for Natural stone test methods (2008). Determination of water absorption at atmospheric pressure.
[38] ASTM C97-96 Standard Test Methods for Absorption and Bulk Specific Gravity of Dimension Stone, (2000), ASTM International, West Conshohocken, PA, https://doi.org/10.1520/C0097-96E01.
[39] The European Standard CEN – EN 16322 (2013), Conservation of Cultural Heritage – Test methods – determination of drying properties.
[40] ASTM D3359-02: Standard Test Methods for Measuring Adhesion by Tape Test, (2002), ASTM International, 10 August.
[41] P. Tiano, Rodrigues J. Delgado, E. De Witte, et al., The conservation of monuments: a new method to evaluate consolidating treatments, Int. J. Restor. Build. Monuments 6 (2) (2000) 133–150.
[42] A.P. Pinto, J. Delgado-Rodrigues, Stone consolidation: the role of treatment procedures, J. Cult. Heritage 9 (2008) 38–53.
[43] C.M. Grossi, P. Blimblecombe, R.M. Esbert, et al., Color changes in architectural limestones from pollution and cleaning, Color Res. Appl. 32 (2007) 320–331.
[44] ASTM 6154-4. Standard Test Method for the Accelerated Weathering test Method for QUV QUV/BASIC Weathering Tester.
[45] G. Taglieri, B. Felice, V. Daniele, et al., Analysis of the carbonation process of nanosized $Ca(OH)_2$ particles synthetized by exchange ion process, Proc. Inst. Mech. Eng., Part N: J. Nanoeng. Nanosystems (2014), https://doi.org/10.1177/1740349914537616.
[46] G. Ziegenbald, Colloidal calcium hydroxide – a new material for consolidation and conservation of carbonate stone, Torun, 2008, pp. 1109–1115.
[47] G. Borsoi, B. Lubelli, R. van Hees et al., Deposition of modified nanolimes within calcareous substrates, in: 1-2. Abstract from Green Conservation of Cultural Heritage, Rome, Italy, (2015) 27–28.
[48] R. Giorgi, L. Dei, P. Baglioni, A new method for consolidating wall paintings based on dispersions of lime in alcohol, Stud. Conserv. 45 (3) (2000) 154–161.
[49] M. Ukrainczyk, M. Greiner, E. Elts, et al., Simulating preferential sorption of tartrate on prismatic calcite surfaces, CrystEngComm J. 17 (2015) 149–159, https://doi.org/10.1039/c4ce01447b.
[50] A.E. Charola, E. Wendler, An overview of the water-Porous building materials interactions, Restor. Build. Monuments J. 21 (2–3) (2015) 55–63.
[51] A.E. Charola, E.P. Vicenzi, C.A. Grissom, et al., Composition and characteristics of Kasorta limestons on the exterior of the National Museum of the American Indian, Building. (2017) 17–26;
J. Sledge, A.E. Charola, P.T. De Priest, R. Koestler, eds. Conservation of the Exterior of the National Museum of the American Indian Building, Smithsonian Contributions to Museum Conservation, No. 6. ISSN 1949–2359.
[52] A.E. Charola, Chemical-physical factors in stone deterioration, Durability of Building Materials 5 (1988) 309–316.